Numerical Simulations on the PSP Rotor Using HMB3

A. Jimenez-Garcia[a], G. N. Barakos[b]
CFD Laboratory, School of Engineering, University of Glasgow, G12 8QQ Glasgow, UK

This work presents CFD analyses of the isolated Pressure Sensitive Paint (PSP) model rotor blade in hover and forward flight using the structured multi-block CFD solver of Glasgow University. In hover, two blade-tip Mach numbers (0.585 and 0.65) were simulated for a range of blade pitch angles using fully-turbulent flow and the k-ω SST model. Results at blade-tip Mach number of 0.585 showed a fair agreement with experimental Figure of Merit and surface pressure coefficients obtained in the Rotor Test Cell (RTC) at NASA Langley Research Center. Comparisons are presented at blade-tip Mach number of 0.65 in terms of integral blade loads, surface pressure coefficients and position of the tip-vortex cores with published numerical data. Finally, the flow around the PSP rotor in forward flight was also computed at medium thrust (C_T=0.006) and results were compared with published experimental data.

Nomenclature

$\bar{Q}$	=	$\bar{Q}$-criterion
$\boldsymbol{R}$	=	flow equation residual vector
$\boldsymbol{W}$	=	flow solution vector
a_∞	=	freestream speed of sound, *m/s*
c	=	rotor blade chord
c_{ref}	=	reference blade chord
C_P	=	blade sectional pressure coefficient, $C_P = \dfrac{P - P_\infty}{1/2\rho_\infty(\Omega r)^2}$
C_P^*	=	critical pressure coefficient
C_Q	=	rotor torque coefficient, $C_Q = \dfrac{Q}{\rho_\infty(\Omega R)^2 \pi R^3}$
C_q	=	blade sectional torque coefficient, $C_q = \dfrac{\mathrm{d}C_Q}{\mathrm{d}r}$
C_Q/σ	=	blade torque coefficient, torque coefficient divided by rotor solidity

[a] PhD Candidate, CFD Laboratory, School of Engineering, Email: a.jimenez-garcia.1@research.gla.ac.uk
[b] Professor, MAIAA, MRAeS, CFD Laboratory, School of Engineering, Email: George.Barakos@glasgow.ac.uk

C_t = blade sectional thrust coefficient, $C_t = \dfrac{\mathrm{d}C_T}{\mathrm{d}r}$

C_T = rotor thrust coefficient, $C_T = \dfrac{T}{\rho_\infty(\Omega R)^2\pi R^2}$

C_T/σ = blade loading coefficient, thrust coefficient divided by rotor solidity

C_{DO} = overall profile drag coefficient

k = turbulent kinetic energy

k_i = induced power factor

M^2C_m = pitching moment coefficient

M^2C_n = normal force coefficient

M_{tip} = blade-tip Mach number, $M_{\text{tip}} = \dfrac{V_{\text{tip}}}{a_\infty}$

N_{b} = number of blades

P = pressure

P_∞ = freestream pressure

Q = rotor torque

R = rotor radius

r = radial coordinate along the blade span

Re = Reynolds number, Re $= V_{\text{tip}}c_{\text{ref}}/\nu_\infty$

S_{ij} = symmetric part of the velocity gradient

T = rotor thrust

V_{tip} = blade-tip speed, $V_{\text{tip}} = \Omega R$

FoM = figure of merit, FoM = $\dfrac{C_T^{3/2}}{\sqrt{2}C_Q}$

α_{shaft} = shaft angle, *deg*

μ = advance ratio, M_∞/M_{tip}

ν_∞ = freestream kinematic viscosity

Ω = rotor rotational speed

Ω_{ij} = antisymmetric part of the velocity gradient

Ψ = azimuth angle

ρ_∞ = freestream density

σ = rotor solidity, $\sigma = \dfrac{N_b c_{\text{ref}}}{\pi R}$

Θ = local blade twist angle

θ_{75} = blade pitch angle at r/R = 0.75

ξ = vorticity, *rad/s*

ABS = advanced blade side

ADD = aviation development directorate

ALE = arbitrary Lagrangian Eulerian

BET = blade element theory

BILU = block incomplete lower upper

BSL = Menter baseline

CFD = computational fluid dynamics

CFL = Courant Friedrichs Lewy

DDES = delayed detached eddy simulation

DES = detached eddy simulation

GRMS = general rotor model system

HMB = helicopter multi-block

LES = large eddy simulation

MUSCL = monotone upstream centered schemes for conservation laws

NFAC = NASA Ames full-scale aerodynamics complex

OGE = out-of-ground effect

PIV = particle image velocimetry

PSP = pressure sensitive paint

RANS = Reynolds averaged Navier-Stokes

RBS = retreating blade side

ROBIN = rotor body interaction fuselage

RTC = rotor test cell

SA = Spalart Allmaras

SST = shear stress transport

∞ = freestream value

tip = blade-tip value

* = sonic condition

I. Introduction

With work on the S-76 rotor and XV-15 tiltrotor blades providing encouraging results regarding the prediction of integral loads with CFD in hover [1, 2], the PSP rotor is now analysed. Regarding the XV-15 rotor, the transition onset and distribution of skin friction were well predicted and were found to have a mild effect on the overall figure of merit [2]. These works also showed the potential of transport-based models for transition prediction in complex 3D flows.

One of the main limitation to completely validate CFD methods using the S-76 and XV-15 blades was the lack of surface pressure data. In this regard, a model-scale known as Pressure Sensitive Paint (PSP) rotor was designed jointly by the NASA Langley Research Center and the U.S. Army Aviation Development Directorate (ADD) and manufactured in 2002. The blade has so far been used for experiments to compare PSP data with measurements using Kulite pressure transducers [3–5] in the Rotor Test Cell (RTC) at the NASA Langley Research Center 14$\times$22 Foot Subsonic Wind Tunnel, and is to be re-used for further tests in hover at blade-tip Mach number of 0.65 as part of a future campaign that will be conducted in the NASA Ames Full-Scale Aerodynamics Complex (NFAC) 80$\times$120 Foot Wind Tunnel.

In this work, we present an aerodynamic study of the PSP blades with high-fidelity computational fluid dynamics. The first part of this work is devoted to hover computations. In this regard, two blade-tip Mach numbers (0.585 and 0.65) were simulated for a range of blade pitch angles using the fully-turbulent k-ω SST model. The aim is to assess the level of accuracy of the present CFD method in predicting the Figure of Merit. This is addressed by comparing with experimental data available in the literature [3, 4, 6] for the lower blade-tip Mach number 0.585. Moreover, the effects of turbulence models and mesh density on the Figure of Merit were also studied. Regarding the blade-tip Mach number of 0.65, a detailed analysis of the performance of the isolated PSP is shown, where results are presented for a range of design points, which include medium and high thrust hover conditions and comparisons with available CFD data. To reduce the computational cost, the hover flow is solved by casting the equations as a steady-state problem in a noninertial reference frame.

The second part of this paper presents numerical simulations of the PSP rotor in forward flight at an advance ratio of $\mu = 0.35$ and thrust coefficient of $C_T = 0.006$. For this case, we solved the forward flight flow by casting the problem as unsteady and using the overset grid method. The predicted surface pressure coefficient at $r/R = 0.99$ at the Advanced Blade Side (ABS, $\Psi = 101°$) and the Retreating Blade Side (RBS, $\Psi = 262°$) are reported and compared with available experimental data [4].

II. CFD Method

A. HMB Solver

The Helicopter Multi-Block (HMB) [7, 8] code is used as the CFD solver for the present work. It solves the Unsteady Reynolds Averaged Navier-Stokes (URANS) equations in integral form using the Arbitrary Lagrangian Eulerian (ALE) formulation for time-dependent domains, which may include moving boundaries. The Navier-Stokes equations are discretised using a cell-centred finite volume approach on a multi-block grid. The spatial discretisation of these equations leads to a set of ordinary differential equations in time,

$$\frac{d}{dt}(\boldsymbol{W}_{i,j,k}\, V_{i,j,k}) = -\boldsymbol{R}_{i,j,k}(\boldsymbol{W}) \tag{1}$$

where i, j, k represent the cell index, $\boldsymbol{W}$ and $\boldsymbol{R}$ are the vector of conservative flow variables and flux residual respectively, and $V_{i,j,k}$ is the volume of the cell i, j, k. To evaluate the convective fluxes, the Osher[9] approximate Riemann solver is used, while the viscous terms are discretised using a second order central differencing spatial discretisation. The Monotone Upstream-centred Schemes for Conservation Laws, which is referred to in the literature as the MUSCL approach and developed by Leer [10], is used to provide high-order accuracy in space. The HMB solver uses the alternative form of the Albada limiter [11] being activated in regions where a large gradients are encountered mainly due to shock waves, avoiding the non-physical spurious oscillations. An implicit dual-time stepping method is employed to performed the temporal integration, where the solution is marching in pseudo-time iterations to achieve fast convergence, which is solved using a first-order backward difference. The linearised system of equations is solved using the Generalised Conjugate Gradient method with a Block Incomplete Lower-Upper (BILU) factorisation as a pre-conditioner [12]. To allow an easy sharing of the calculation load for parallel job, a multi-block structured meshes are used. Various turbulence models are available in HMB solver, including several one-equation, two-equation, three-equation, and four-equation turbulence models. Furthermore, Large-Eddy Simulation (LES), Detached-Eddy Simulation (DES) and Delay-Detached-Eddy Simulation (DDES) are also available. For this study, the fully-turbulent Wilcox's k-ω model [13] and the k-ω BSL and SST models from Menter [14] are employed.

1. Overset Grid Method

Overset grids and sliding plane methods are available in HMB [8, 15] to allow for the relative motion between different mesh components. Both methods have been employed for isolated rotor blades, such as the UH-60A by Dehaeze *et al.* [16], the S-76 by Jimenez-Garcia *et al.* [17], the XV-15 by Gates [18] and

even for complete helicopter configurations [8]. For the present work, an overset grid method is employed to ease the generation of each individual mesh component for hover computations, and to allow for the relative motion between mesh components in forward flight cases.

The overset grid method, also referred to as the chimera method, is based on structured composite grids with hexahedral elements, consisting of independently generated, overlapping non-matching sub-domains. A hierarchical approach is employed allowing to interpolate the solution variables based on an user-specified hierarchy of sub-domains. The interpolation between composite grids depends on a localisation procedure, that includes a localisation pre-processing and a chimera search which aim is to minimise the number of searches due to potential mesh overlap. Three methods are available to control the interpolation needed for the chimera solution; zero order single-neighbour, inverse distance, and variable-distribution reconstruction-based interpolation. Further information about the implementation of the overset grid method in HMB can be found in [15].

III. Rotor Geometry and Mesh Generation

A. PSP Rotor Geometry

The four-bladed PSP rotor has an aspect ratio (R/c) of 12.2 and a nominal twist of -14 degrees. The main characteristics of the rotor blades are summarised in Table 1. The blade planform has been generated using three radial stations. First, the RC(4)-12 aerofoil was used up to 65% R. Then, the RC(4)-10 aerofoil from 70% R to 80% R. Finally, the RC(6)-08 aerofoil was used from 85% R to the tip. The aerodynamic characteristics of these aerofoils can be found in [19, 20]. The planform of the PSP model rotor has a 60% tapered and 30° swept tip and the details on the blade radial twist and the chord distributions are shown in Figure 1.

Parameter	Value
Number of blades (N_b)	4
Rotor radius (R)	66.50 inches
Rotor blade chord (c)	5.45 inches
Aspect ratio (R/c)	12.2
Rotor solidity (σ)	0.1033
Linear twist angle (Θ)	-14°

Table 1: Geometric properties of the PSP rotor [5].

B. PSP Rotor Mesh

As already mentioned, the chimera technique is used for the aerodynamic study of the PSP rotor. For hover computations, only a quarter of the computational domain was meshed, assuming periodic conditions for the flowfield in the azimuthal direction. This assumption is valid if the wake generated by the rotor is assumed periodic and the blades do not experience stall. A view of the computational domain along with the employed boundary conditions is given in Figure 2. For the blades, a C-topology around the leading edge of

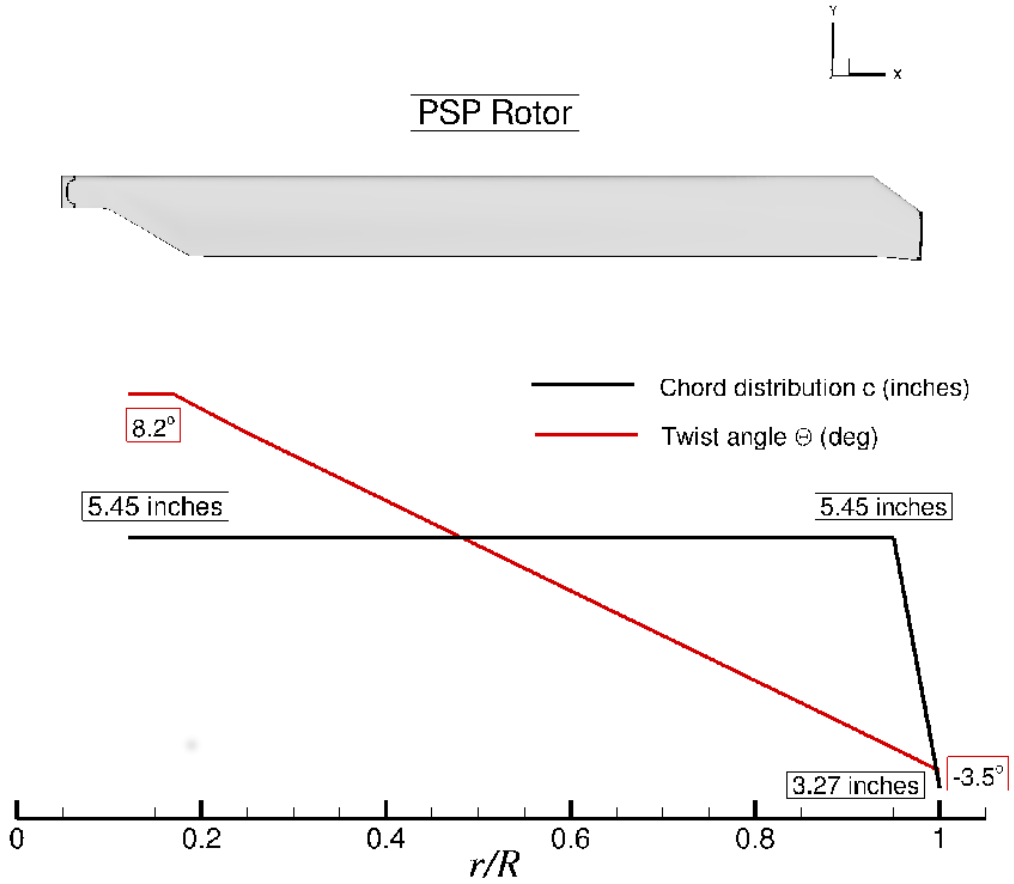

Fig. 1: Geometry of the PSP model rotor with 60% taper and 30° swept tip [5].

the blade was selected, whereas an H-topology was employed at the trailing edge [2]. To assess the effect of the mesh density on the Figure of Merit (hover case), two background grids were built, keeping the same number of points around the PSP blade.

The multi-block structured grid for the PSP rotor in forward flight has a total of 61.6 million cells with 1968 blocks, with 50 and 11.6 million cells for the background and body-fitted grids, respectively. A hub is also included in the computational domain and modelled as a generic ellipsoidal surface. The meshing parameters for the PSP mesh rotor blade along with the grids used for hover and forward flight cases are shown in Table 2.

IV. Test Conditions and Computations

In hover, the PSP blade was simulated at two blade-tip Mach numbers, corresponding to 0.585 and 0.65. As a means to validate the pressure sensitive paint (PSP) technique for rotor blades in hover, Wong *et al.* [3] measured C_P at two radial stations at blade-tip Mach number of 0.585 on the PSP rotor blades, which were installed on the modified ROtor BOdy Interaction fuselage (ROBIN Mod7). Recently, Overmeyer *et al.* [6] extended this hover tests, measuring integrated blade loads for free and fixed transition and transition

	Mesh I (hover)	Mesh II (hover)	Mesh III (forward flight)
Background mesh size (cells)	7.2 million	3.1 million	50 million
Blade mesh size (cells)	5.2 million	5.2 million	11.6 million (four blades)
Overall mesh size (cells)	12.4 million	8.3 million	61.6 million
Wall distance	$1.0 \cdot 10^{-5} c_{\text{ref}}$	$1.0 \cdot 10^{-5} c_{\text{ref}}$	$1.0 \cdot 10^{-5} c_{\text{ref}}$
Points along the span	215	215	145
Points around the aerofoil	252	252	270

Table 2: Meshing parameters for the PSP rotor mesh.

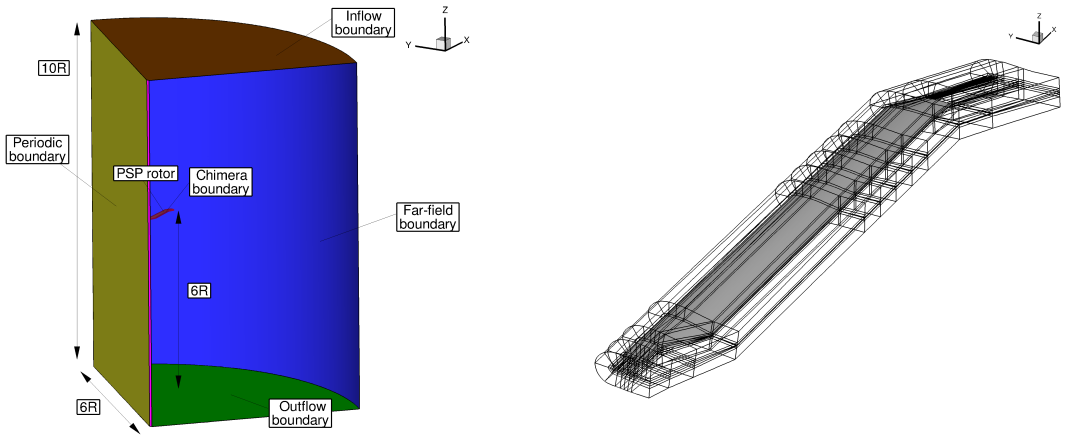

(a) Computational domain.

(b) PSP rotor mesh.

Fig. 2: Computational domain and boundary conditions employed (left) and topology of the PSP rotor mesh (right).

locations using the same conditions in the same facility (Rotor Test Cell at the NASA Langley Research Center 14×22 Foot Subsonic Wind Tunnel). This hover condition is simulated here in out-of-ground effect (OGE) conditions for six blade pitch angles. Moreover, the effect of turbulence models on the integrated loads is also evaluated at fixed blade pitch angle ($\theta_{75} = 12°$). The Reynolds number, based on the reference blade chord c_{ref} of 5.45 inches and on the blade-tip speed, was $1.05 \cdot 10^6$.

A future campaign of tests in hover on the PSP rotor blade will be conducted in the NASA Ames Full-Scale Aerodynamics Complex (NFAC) 80×120 Foot Wind Tunnel, where the effect of the facility on the performance and transition point will be reported. Also, visualisation of the flowfield using Particle Image Velocimetry (PIV) is planned at a higher blade-tip Mach number of 0.65. Thus, results are presented here in terms of integral blade loads, surface pressure coefficients, position of the tip-vortex cores, and wake visualisation, where the blade-tip Mach number was set to 0.65, and seven collective angles were considered, covering low, medium, and high disc loadings. The effect of the mesh density (Meshes I and II of Table 2) on the Figure of Merit is also reported. As a means of comparing integrated loads at the same thrust coefficient, a fixed thrust was computed corresponding to C_T/σ=0.085. The Reynolds number, based on the reference blade chord of 5.45 inches and on the tip speed, was $2.16 \cdot 10^6$. All flow solutions were computed by solving

the RANS equations, coupled with either Wilcox's k-ω model [13] or Menter's $k-\omega$ (BSL or SST) turbulence model [14]. The flow equations were integrated with the implicit dual-time stepping method of HMB, using a pseudotime Courant–Friedrichs–Lewy (CFL) equal to 4.

The PSP main rotor was also simulated at medium-speed forward flight. Flight test data for this case was acquired by Wong *et al.* [4] at the 14-by 22-ft Subsonic Tunnel at the NASA Langley Research Center on the General Rotor Model System (GRMS) test stand [21]. The rotor advance ratio was $\mu = 0.35$, and the freestream Mach number was 0.2. To meet the target thrust coefficient (blade loading coefficient $C_T = 0.006$) while having zero roll and pitch moments, a matrix trimming method is used in HMB [7], based on the Blade Element Theory (BET) for computing the elements of the sensitivity matrix. The flow solutions were computed solving the URANS equations, coupled with Menter's k-ω SST turbulence model [14]. The employed time step corresponds to 0.25 deg in the azimuthal direction and was based on experience gained with previous rotor computations in forward flight [8].

Table 3 summarises the employed conditions and the computations performed. The values of blade pitch and coning angles alongside thrust coefficient and turbulence model (TM in Table 3) employed are also reported.

ID	**Test case (Mesh)**	$\mathbf{M}_{\text{tip}}$	$\mathbf{M}_\infty$	$\theta_{\mathbf{75}}(\mathbf{deg})$	$\beta(\mathbf{deg})$	C_T	**TM**
1	Hover (Mesh I)	0.585	0	4°	0°	0.00259	SST
2	Hover (Mesh I)	0.585	0	6.58°	1.39°	0.00503	SST
3	Hover (Mesh I)	0.585	0	8.48°	2.44°	0.00694	SST
4	Hover (Mesh I)	0.585	0	9.46°	3.02°	0.00797	SST
5	Hover (Mesh I)	0.585	0	10.3°	3.5°	0.00893	SST
6	Hover (Mesh I)	0.585	0	12°	0°	0.01059	SST
7	Hover (Mesh I)	0.585	0	12°	0°	0.01060	BSL
8	Hover (Mesh I)	0.585	0	12°	0°	0.01062	Wilcox
9	Hover (Mesh I)	0.65	0	6°	0°	0.00451	SST
9(1)	Hover (Mesh II)	0.65	0	6°	0°	0.00458	SST
10	Hover (Mesh I)	0.65	0	7°	0°	0.00552	SST
11	Hover (Mesh I)	0.65	0	8°	0°	0.00657	SST
12	Hover (Mesh I)	0.65	0	9°	0°	0.00767	SST
12(1)	Hover (Mesh II)	0.65	0	9°	0°	0.00771	SST
13	Hover (Mesh I)	0.65	0	10°	0°	0.00881	SST
14	Hover (Mesh I)	0.65	0	11°	0°	0.00985	SST
15	Hover (Mesh I)	0.65	0	12°	0°	0.01095	SST
15(1)	Hover (Mesh II)	0.65	0	12°	0°	0.01106	SST
16	Hover (Mesh I)	0.65	0	9.92°	3.09°	0.0875	SST
17	FF (Mesh III)	0.585	0.2	8.32°	3.28°	0.006	SST

Table 3: Computational cases for the PSP rotor. TM=Turbulence model; FF=Forward flight; BSL=Baseline k-ω [14]; SST=Shear Stress Transport [14].

V. Results and Discussions

The first cases considered here correspond to the hover case at lower blade-tip Mach number 0.585 (A) and at blade-tip Mach number 0.65 (B). The PSP rotor in forward flight at advance ratio of 0.35 and $C_T = 0.006$ is presented in section (C).

A. PSP in Hover: Blade-tip Mach number of 0.585

1. Integrated Blade Loads

Figure 3 shows the variation of FoM and torque coefficient with the blade loading coefficient, at six blade pitch angles, covering low, medium, and high thrust (see Table 3). Comparison with experimental data (opened squares) by Overmeyer *et al.* [6] for the fixed-transition, 5% c, upper and lower (run 156) and momentum-based estimates of the Figure of Merit (dashed lines) are also included. For the momentum-theory curve, and induced power factor k_i of 1.15 and overall profile drag coefficient C_{D0} of 0.01 were selected. Three sets of published CFD simulations are also included for direct comparison. Green lines correspond to Wong [22], using the unstructured solver FUN3D and the fixed Spalart-Allmaras as turbulence model [23]. Vieira *et al.* [24] employed the commercial software Star-CCM+ (red triangle symbols) with the same turbulence model. Blue diamond symbols correspond to numerical simulations performed by Rohit [25] with the structured OVERFLOW solver, fully turbulent and isolated rotor (without fuselage) (see Rohit [25], Figure 10). Note that the experiments reported here does not correspond to the isolated PSP rotor, thus some degree of discrepancy on the airloads is expected.

At low thrust $C_T/\sigma < 0.06$, it can be seen that all CFD computations are in close agreement with the experimental data. Note that at low thrust, FoM shows low values as consequence of the higher contribution of the profile drag, which is relatively easy to predict. At medium and high thrust $0.06 < C_T/\sigma < 0.1$, results with FUN3D, OVERFLOW and Star-CCM+ over-predict the values of FoM, while HMB3 shows an under-predicted FoM. As an example, at thrust coefficient of $C_T/\sigma = 0.0828$, FUN3D, OVERFLOW, Star-CCM+, and HMB3 shows a discrepancy of +1.7,+0.8,+2.5, and -0.4 counts of FoM respect to the experiments. Note that the OVERFLOW and FUN3D values reported here were extracted from the papers ([25], Figure 10) and ([22], Figure 18), respectively, which may introduce a source of discrepancy when compared. Regarding the maximum thrust coefficient measured in the wind tunnel $C_T/\sigma < 0.096$, HMB3 results show maximum discrepancies of -2 counts with respect to the experiments. Rohit ([25], Figure 10) evaluated the effect of rotor installation on the FoM, and it was found that the installed-rotor FoM presents a higher values (around 1.4 counts of FoM) when compared with the isolated rotor at $C_T/\sigma \approx 0.094$, which perhaps is one of the source of discrepancy at high thrust between HMB3 and experiments results. Despite the good correlation with the FoM and torque coefficient with the experiments, this work needs to be extended to include the fuselage and unsteady computations in addition to the steady-state results presented here as means to gain a better insight of the PSP performance at high thrust.

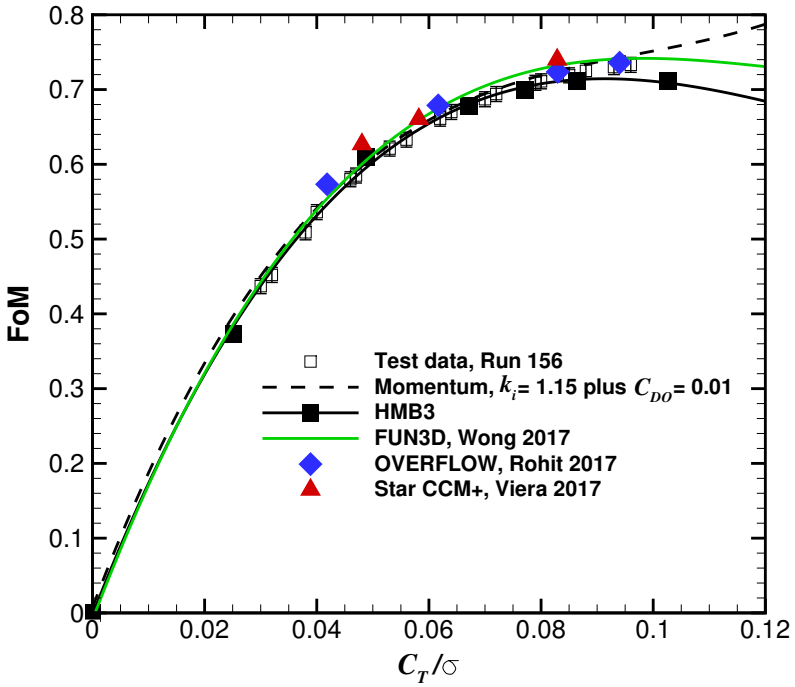

(a) C_T/σ-FoM.

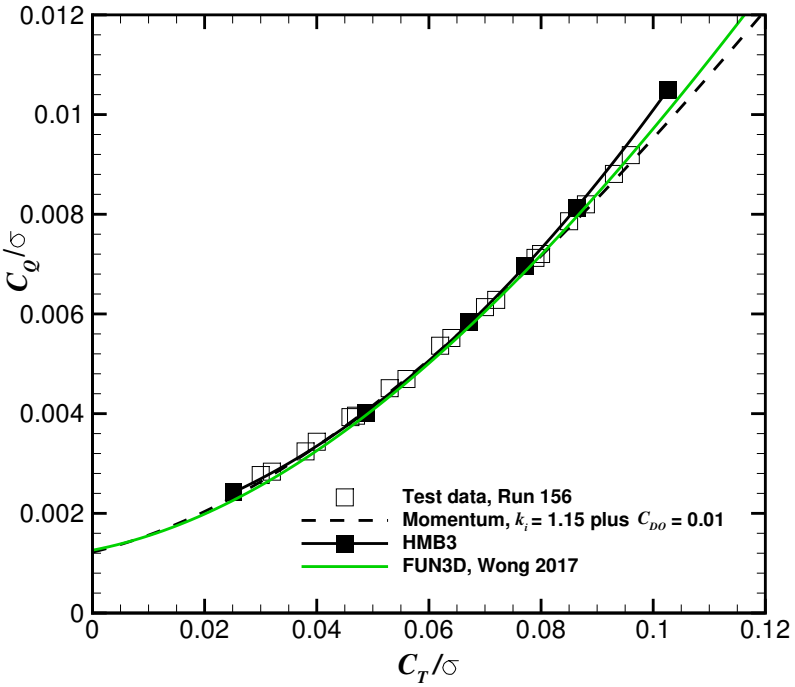

(b) C_T/σ-C_Q/σ.

Fig. 3: Integrated blade loads for the PSP model rotor at blade-tip Mach number of 0.585. Comparisons with published CFD data: FUN3D [22] (green lines), OVERFLOW [25] (blue diamond symbols), Star CCM+ [24] (red triangle symbols) and experimental data [6] (opened square symbols) are also shown.

The effect of three fully-turbulence models on the Figure of Merit at high thrust coefficient (fixed blade pitch angle of $\theta_{75} = 12°$) is shown in Table 4. Even though the thrust coefficient was not trimmed, less than 0.25% discrepancy was found between the employed turbulence models. For this case, the FoM does not seem to be affected by the use of the turbulence model, with a maximum peak-to-peak of 0.13 counts of FoM.

Turbulence Model	$\mathbf{C_T}/\sigma$	$\mathbf{C_Q}/\sigma$	**FoM**
k-ω Wilcox [13]	0.10285	0.010531	0.7118
k-ω Menter (BSL) [14]	0.10270	0.010497	0.7125
k-ω Menter (SST) [14]	0.10259	0.010501	0.7112

Table 4: Effect of the turbulence model on the C_T/σ, C_Q/σ, and FoM for the PSP rotor at blade-tip Mach number of 0.585 and blade pitch angle of $12°$.

2. Surface Pressure Predictions

Surface pressure coefficients (C_P) are compared between CFD and experimental data [3, 4] at two radial stations (r/R= 0.93 and 0.99) on the upper surface of the PSP blade on the Mesh I (see Table 2) and using the k-ω SST turbulence model. The C_P is computed based on the local velocity at each radial station:

$$C_P = \frac{P - P_\infty}{1/2\rho_\infty(\Omega r)^2}. \tag{2}$$

Regarding the experiments, two techniques were used to measured C_P distributions, the traditional transducers Kulite (square symbols) and the PSP technique (dashed lines) in Figures 4-5. A reasonable agreement is seen by both techniques for both stations at the four thrust coefficients considered here; C_T= 0.005, 0.007, 0.008, and 0.009. CFD results are able to predict the overall distribution of C_P at both stations, and the pressure at the trailing edge are also well captured. It is noticeable that discrepancies appear to be present, when sections at higher thrust are analysed. In fact, the CFD predictions reveal a slightly over-predicted C_P, even if the pressure at the trailing edge is well captured.

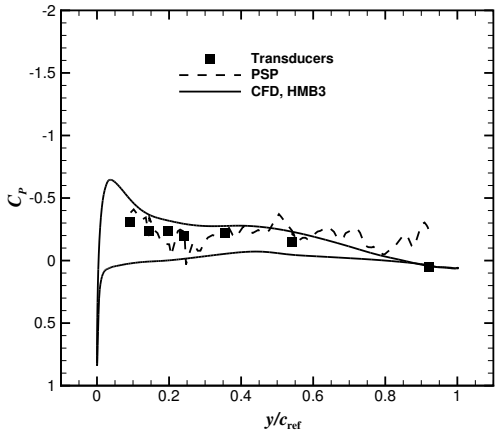

(a) C_T= 0.005.

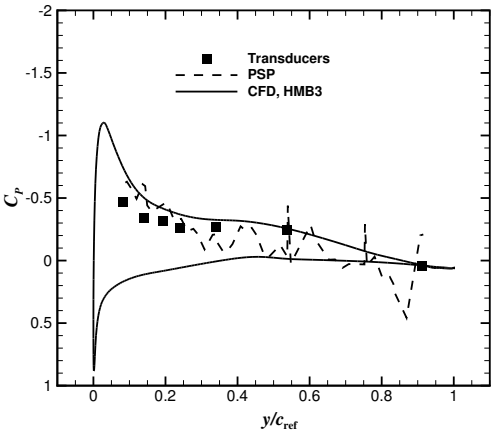

(b) C_T= 0.007.

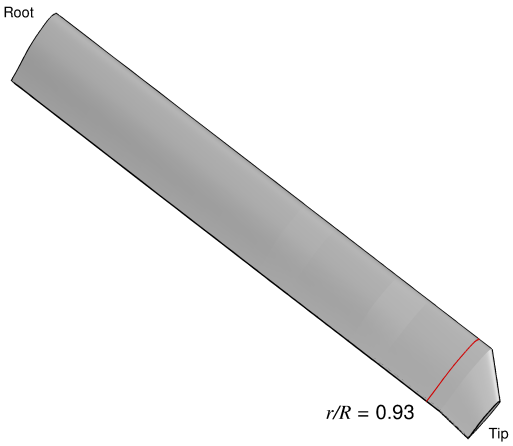

(c) Radial station.

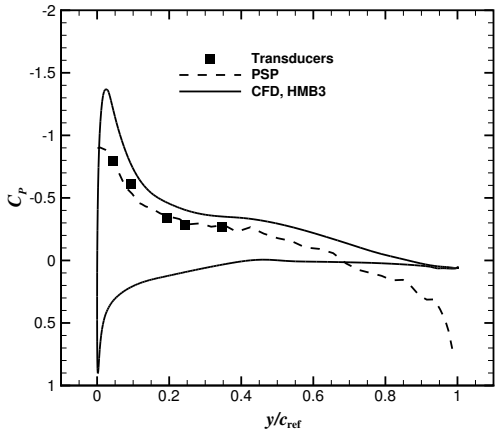

(d) C_T= 0.008.

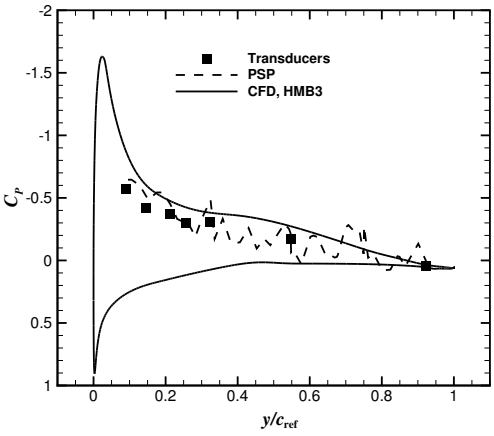

(e) C_T= 0.009.

Fig. 4: C_P profile comparisons between experimental data using the PSP technique (dashed line) and pressure tap (square symbols) [3, 4] and CFD (solid line) at radial station $r/R = 0.93$.

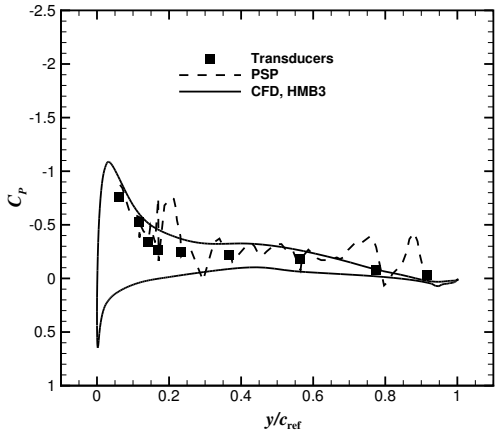

(a) C_T= 0.005.

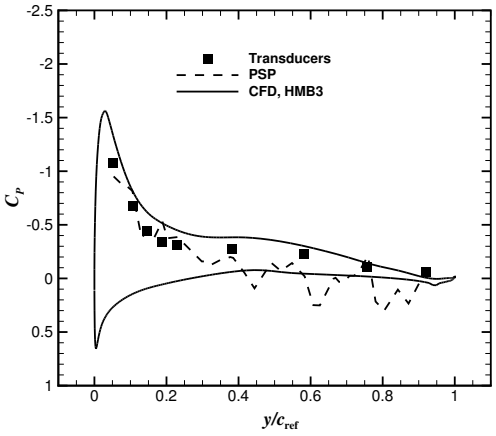

(b) C_T= 0.007.

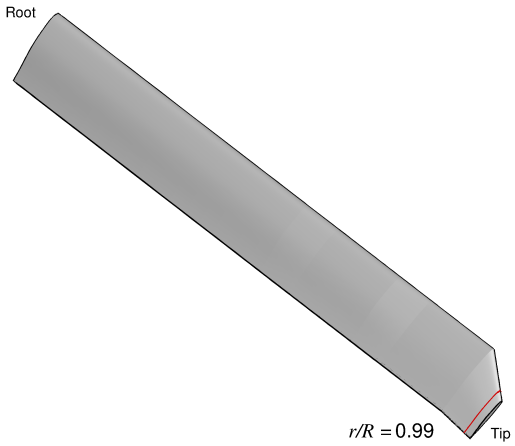

(c) Radial station.

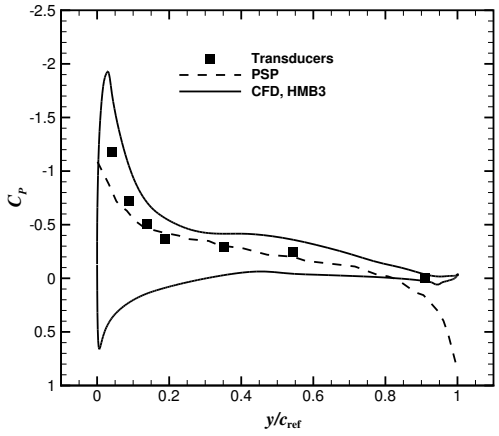

(d) C_T= 0.008.

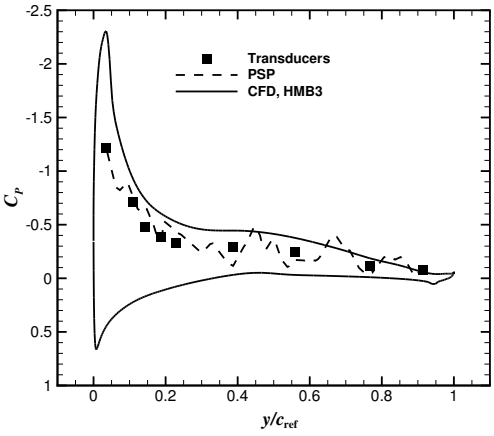

(e) C_T= 0.009.

Fig. 5: C_P profile comparisons between experimental data using the PSP technique (dashed line) and pressure tap (square symbols) [3, 4] and CFD (solid line) at radial station $r/R = 0.99$.

B. Blade-tip Mach number of 0.65

Unlike the PSP blade at lower blade-tip Mach number of 0.585, no experimental data is available for this hover condition. Therefore, we compare the integrated blade loads with published CFD work by Coder [26] and Rohit [25] using the structured OVERFLOW CFD solver with fully turbulence models. Surface pressure coefficients are also shown for various blade pitch angles. To evaluate the accuracy of the CFD predictions using the same geometry under the same loads, a trimmed case was computed corresponding to $C_T/\sigma = 0.085$ and C_P, position of the tip-vortex cores and wake visualisation are included for future comparisons.

1. Integrated Blade Loads

The effect of the mesh density on the Figure of Merit as a function of the blade loading coefficient C_T/σ is shown in Figure 6, where the overset grids I and II (see Table 2) were employed. The body-fitted mesh was kept constant, while the background level was refined from 3.1 to 7.2 million cells. Table 5 reports the effect of the mesh density on C_T/σ, C_Q/σ, and FoM for the coarse and medium chimera grids, at blade collective angles θ_{75} of 6°, 9°, and 12°. Nevertheless, the grid I is used to investigate the effect of the blade pitch angle as discussed in the following paragraph.

Collective	**Grid I**			**Grid II**		
θ_{75} (deg)	$\mathbf{C_T}/\sigma$	$\mathbf{C_Q}/\sigma$	**FoM**	$\mathbf{C_T}/\sigma$	$\mathbf{C_Q}/\sigma$	**FoM**
6	0.0437	0.00359	0.579	0.0444	0.00363	0.585
9	0.0742	0.00652	0.704	0.0747	0.00653	0.710
12	0.1060	0.00111	0.702	0.1071	0.01121	0.710

Table 5: Effect of the mesh density on the C_T/σ, C_Q/σ, and FoM using the grids I and II of Table 2.

The effect of the blade pitch angle on the FoM for the PSP rotor in hover was also carried out at a blade-tip Mach number of 0.65, from θ_{75}= 6° to 12° with a delta of 1 degree. Figure 7 shows the FoM (above) and blade torque coefficient C_Q/σ (below) as functions of the blade loading coefficient C_T/σ. Momentum-based estimates of the Figure of Merit are also included, with an induced power factor k_i of 1.1, and overall profile drag coefficient C_D of 0.01. No experimental data is available, at present, for further comparisons. CFD results using the OVERFLOW CFD solver by Coder 2017 [26] and Rohit 2017 [25] are represented by red triangle and green diamond symbols, as well as, results obtained with FUN3D by Rohit 2017 [25] in blue symbols are also shown for a code-to-code comparison. Overall, good correlation is found between both CFD results, despite that some discrepancies appear to be present at high thrust coefficient (C_T/σ> 0.1) as consequence of different mesh density, turbulence models, and CFD solvers.

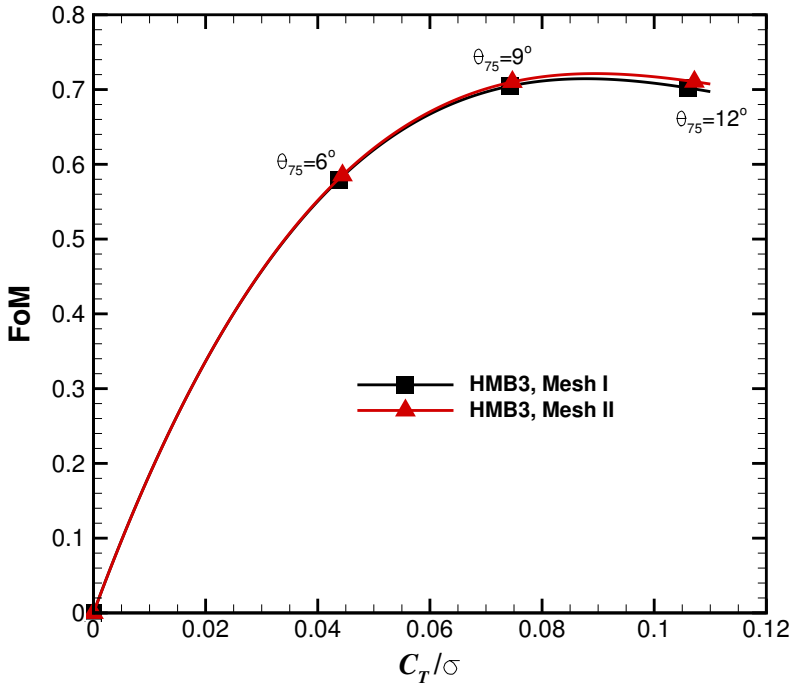

(a) C_T/σ-FoM.

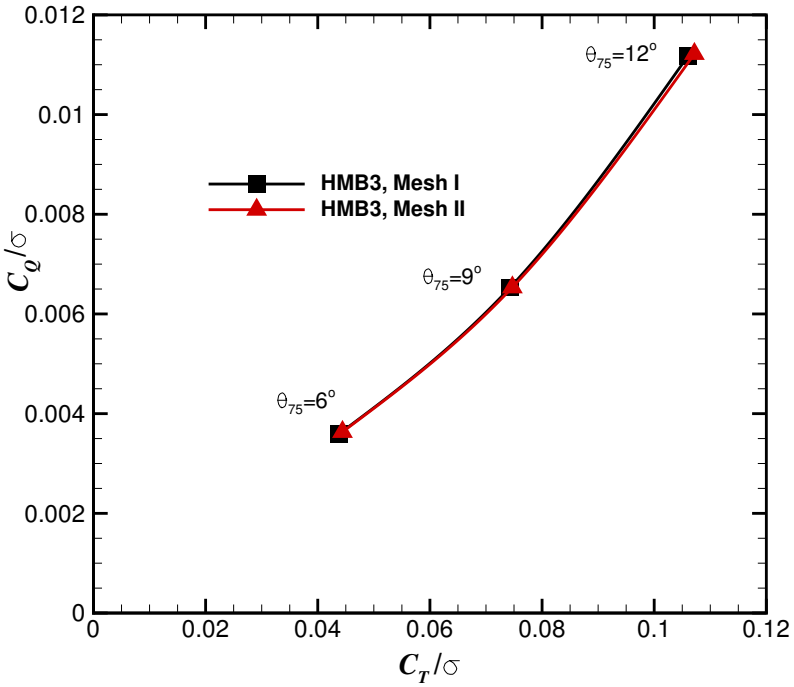

(b) C_T/σ-C_Q/σ.

Fig. 6: Effect of the mesh density on the FoM and C_Q/σ as a function of the C_T/σ for the the PSP model rotor at blade-tip Mach number of 0.65.

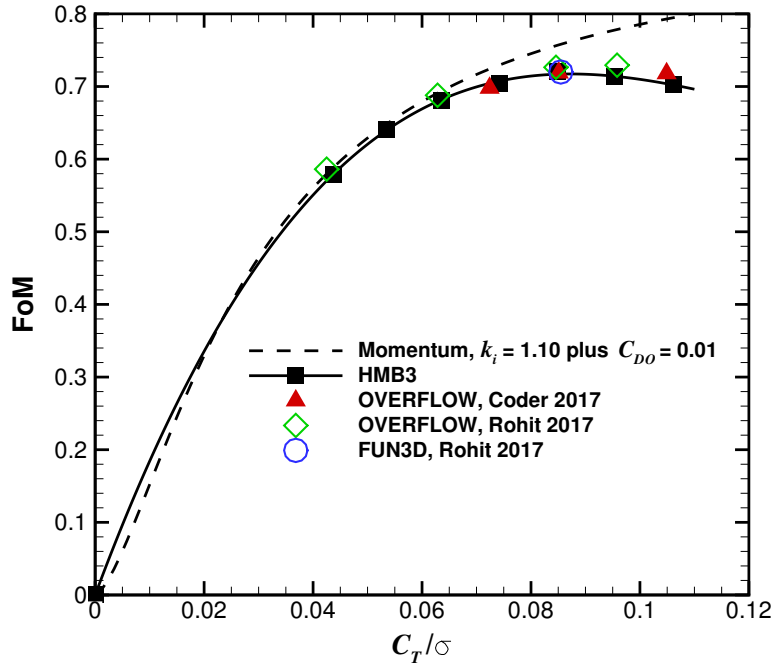

(a) C_T/σ-FoM.

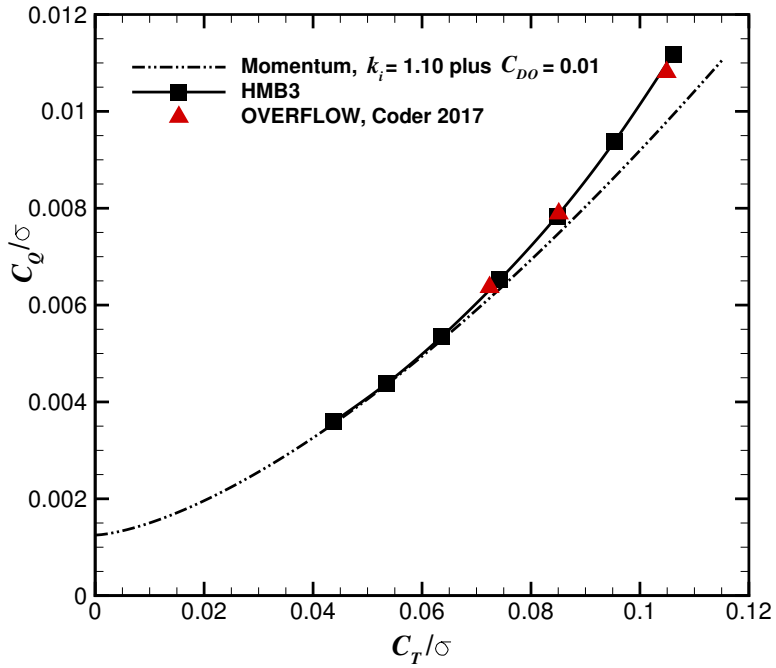

(b) C_T/σ-C_Q/σ.

Fig. 7: Integrated blade loads for the PSP model rotor at blade-tip Mach number of 0.65. Comparison with published CFD data using OVERFLOW by Coder 2017 [26] and Rohit 2017 are represented by red triangle and green diamond symbols, respectively, and FUN3D by Rohit 2017 [25] in blue symbols are also shown.

Four radial stations were considered (r/R= 0.75, 0.85, 0.95, and 0.975), and the blade pitch angles were θ_{75}= 6°, 9°, and 12°. The surface pressure coefficient is computed based on the local velocity at each radial station:

$$C_P = \frac{P - P_\infty}{1/2\rho_\infty(\Omega r)^2}. \tag{3}$$

Regarding the radial station $r/R = 0.75$, it is clear that the suction peak does not exceed the critical C_P^* values, while the most outboard sections (r/R= 0.85, 0.95, and 0.975) reache sonic conditions above 12°, 9°, and 6° of collective, respectively.

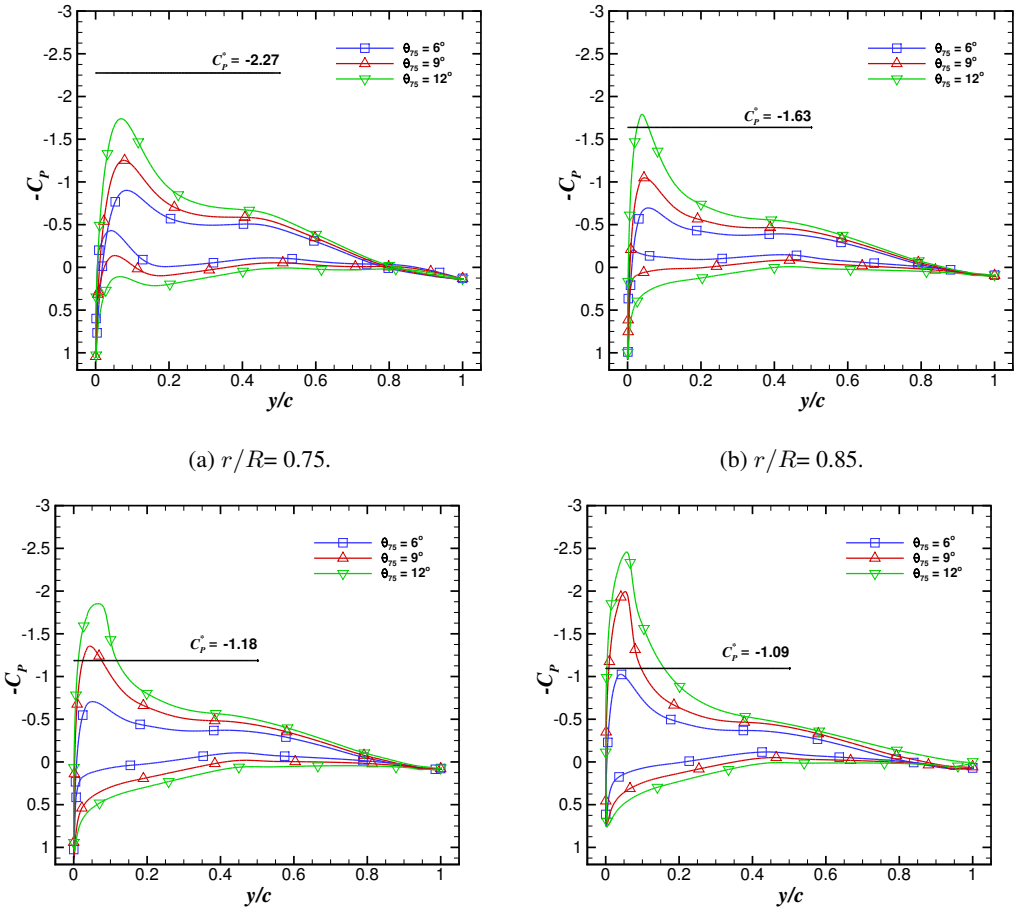

(a) r/R= 0.75.

(b) r/R= 0.85.

(c) r/R= 0.95.

(d) r/R= 0.975.

Fig. 8: C_P profile as function of the blade pitch angle for the PSP model rotor at blade-tip Mach number of 0.65. Radial stations considered: r/R= 0.75, 0.85, 0.95, and 0.975. Critical $C_P^* = \frac{2}{\gamma(M_{\text{tip}}\frac{r}{R})^2}\left[\left(\frac{2+(\gamma-1)(M_{\text{tip}}\frac{r}{R})^2}{\gamma+1}\right)^{\frac{\gamma}{\gamma-1}} - 1\right]$.

3. Trimmed case: C_T/σ=0.085

As previously mentioned, a trimmed case was computed corresponding to $C_T/\sigma = 0.085$ to evaluate the level of accuracy of CFD predictions using the same geometry under the same rotor load. The trim state is specified in Table 6 alongside values of thrust, torque and Figure of Merit for this condition.

Parameter	**Value**
M_{tip}	0.65
θ_{75}	9.92°
β	3.09°
C_T/σ	0.0847
C_T/σ	0.0077
FoM	0.7158

Table 6: Trim state for the PSP rotor in hover at blade-tip Mach number of 0.65 and $C_T/\sigma = 0.085$.

C_P profile for the PSP model rotor at blade-tip Mach number of 0.65 and C_T/σ=0.085 at radial stations r/R= 0.75, 0.85, 0.95, and 0.975 are shown in Figure 9.

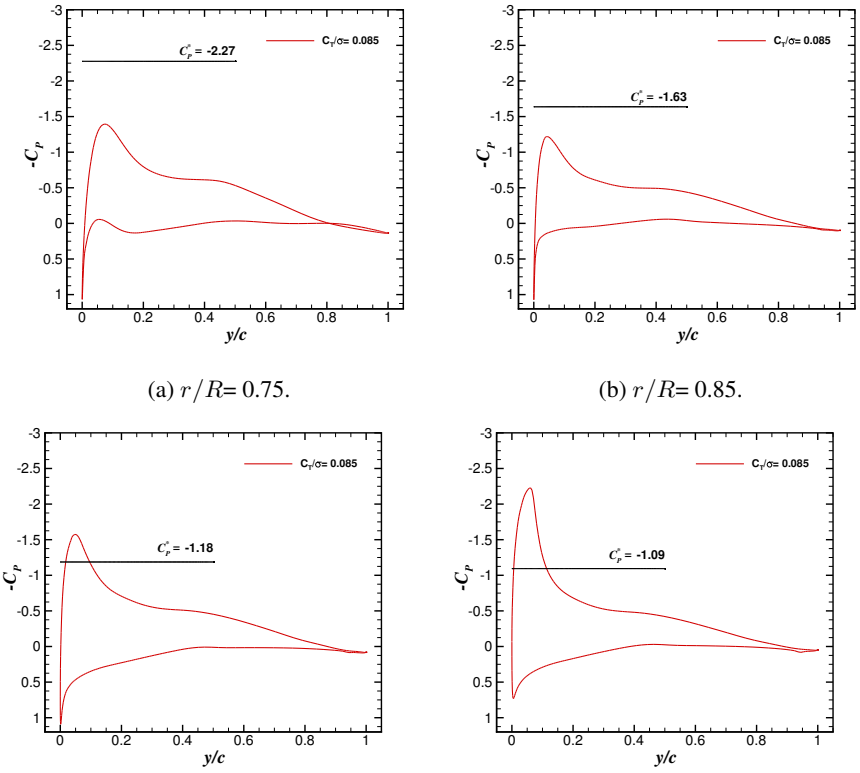

(a) r/R= 0.75.

(b) r/R= 0.85.

(c) r/R= 0.95.

(d) r/R= 0.975.

Fig. 9: C_P profile for the PSP model rotor at blade-tip Mach number of 0.65 and C_T/σ=0.085. Radial stations considered: r/R= 0.75, 0.85, 0.95, and 0.975.

It is well known that to ensure realistic predictions of the wake-induced effects, the radial and vertical displacements of the tip vortex should be resolved, at least for the first and second wake passages [27]. Figure 10 shows a comparison of the (a) radial and (b) vertical displacements of the tip vortices, as functions of the wake age (in degrees), with the prescribed wake-models of Kocurek [28] and Landgrebe [29]. CFD results obtained with the structured CFD solver OVERFLOW by Rohit (see [25], Figure 20) are also reported here (opened square symbols). Both empirical models are based on flow visualisation studies of the rotor wake flow, which is related to the geometric rotor parameters like the number of blades, aspect ratio, chord, solidity, thrust coefficient, and linear twist angle. The prediction of the trajectory, which is captured up to almost 4-blade passages (wake age of 360° for a four-bladed rotor) is in fair agreement with both empirical models and published CFD data [25]. It is found that the radial tip vortex displacement seems to be more sensitive to the change of mesh density that the vertical one, as shown in (Figure 10 (a)). Nevertheless, the CFD results seems to accurately predict the slow convection of the tip vortices (up to wake age of 90°) seen in the vertical displacement (-z/R). This rate is drastically increased as a consequence of the passage of the following blade, leading to a linear increment of the vertical displacement of the wake. These changes are well captured by the present CFD method.

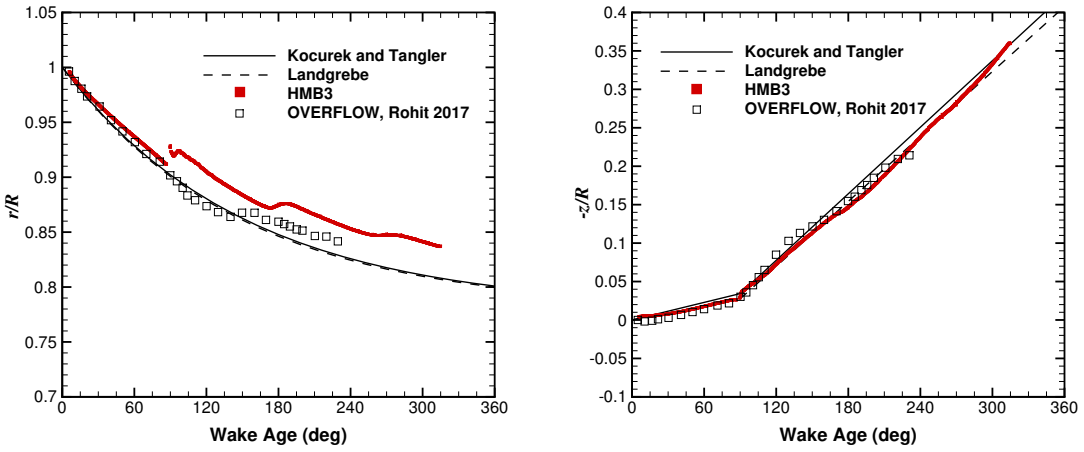

(a) (b)

Fig. 10: Comparison between the radial (left) and vertical (right) tip vortex displacements and the prescribed wake-models of Kocurek and Tangler [28] (solid lines) and Landgrebe [29] (dashed lines). Opened square symbols were obtained with OVERFLOW by Rohit [25]. This case corresponds to the PSP model rotor at blade-tip Mach number of 0.65 and C_T/σ=0.085.

Visualisation of the flowfield of the PSP rotor using the $\bar{Q}$-criterion [30] is presented in Figure 11. The quantity Q is defined as follows:

$$Q = \frac{1}{2}(\Omega_{ij}\Omega_{ij} - S_{ij}S_{ij}), \tag{4}$$

where Ω_{ij} and S_{ij} are the antisymmetric and symmetric part of the velocity gradient tensor, respectively:

$$\Omega_{ij} = \frac{1}{2}\left(\frac{\partial u_i}{\partial x_j} - \frac{\partial u_j}{\partial x_i}\right), \quad S_{ij} = \frac{1}{2}\left(\frac{\partial u_i}{\partial x_j} + \frac{\partial u_j}{\partial x_i}\right). \tag{5}$$

The quantity Q has the dimensions of a velocity squared divided by a length squared, and it is therefore nondimensionalised in HMB as follows:

$$\bar{Q} = Q\left(\frac{L_{\text{ref}}}{V_{\text{ref}}}\right)^2. \tag{6}$$

This informative plot reveals that computations capture the rotor wake up to 4 blade passages for the chimera grid I (see Table 2). Figure 11 (b) shows contours of vorticity magnitude at y= 0. The CFD solution obtained with the medium background grid (7.2 million cells) is able to capture the first four blade passages without a significant dissipation of the vortex core and distortion of its shape. However, the fifth blade passage suffers smearing and distorsion due to the use of lower high-order spatial reconstruction and biased-scheme, respectively. Finally, Figure 11 shows the decay of the vorticity values at the tip core centre as function of the wake age (deg). This quantity appears to be highly influenced by the jump in mesh density between the blade and background grids.

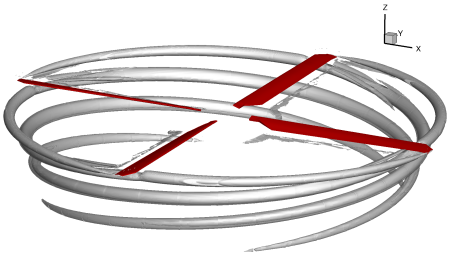

(a) Rotor wake.

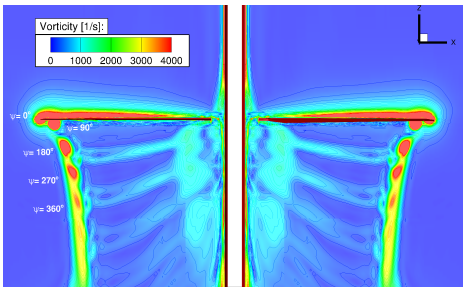

(b) Contours of vorticity magnitude at $y = 0$.

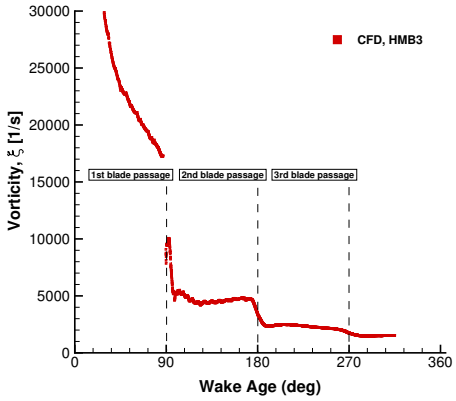

(c) Vorticity values at the tip core centre.

Fig. 11: (a) Visualisation of the flowfield of the PSP rotor using the $\bar{Q}$-criterion, (b) contours of vorticity magnitude at y= 0, and (c) vorticity values at the tip core centre. Blade-tip Mach number is 0.65 and C_T/σ=0.085.

C. PSP Rotor in Forward Flight

The PSP main rotor was also simulated at medium-speed forward flight. Flight test data for this case was acquired by Wong *et al.* [4] at the 14-by 22-ft Subsonic Tunnel at the NASA Langley Research Center on the General Rotor Model System (GRMS) test stand [21]. The rotor advance ratio was μ= 0.35, the freestream Mach number 0.2 and the shaft angle $\alpha_{\text{shaft}} = -6^\circ$. Four thrust conditions were measured by Wong [4], however, a mild thrust coefficient ($C_T = 0.006$) was simulated here. The trim state is specified in Table 7. Note that the negative Fourier series is used with the HMB solver.

Parameter	Value
μ	0.35
M_{tip}	0.58
θ_{shaft}	-6°
θ_0	8.32°
θ_{1s}	6.84°
θ_{1c}	-3.39°
β_0	3.28°
β_{1s}	-0.64°
β_{1c}	-0.77°

Table 7: Trim state for the PSP forward flight case at advance ratio μ =0.35 and $C_T = 0.006$.

Figure 12 shows the normal force and pitching moment on the rotor disk of the PSP. Abrupt reductions of these values (blue) are found at the Advanced Blade Side (ABS) region ($90 < \psi < 180$). Such plots can be very useful to detect stall regions on the rotor [31]. The predicted normal and pitching moment (with the mean values removed) coefficients at six radial stations are reported in Figures 13 and 14. Unfortunately, experimental data is no available for comparison.

Like for the PSP blade in hover, at a blade-tip Mach number of 0.585, experimental surface pressure coefficient are available at the station r/R=0.99 at the ABS and RBS of the rotor. Two techniques were used to measured C_P distributions, the traditional transducers Kulite (square symbols) and the non-intrusive PSP technique (dashed lines) in Figure 15. CFD results were extracted at the ABS ($\psi = 100^\circ$) and RBS ($\psi = 260^\circ$), while experimental C_P were measured at 101° and 262°. Note that the PSP data is sample at the 98.2%R station. Regarding the ABS side, a large discrepancy is seen by both techniques. CFD results are able to predict the overall distribution of C_P and follow quite well the Kulite C_P data. The same behaviour is found at the retreating side where CFD predictions are in close agreement with the Kulite data too.

Finally, visualisation of the PSP rotor flowfield using the $\bar{Q}$-criterion [30] is presented in Figure 16. The CFD results appear to capture well the main flow structures near and far the rotor disk. Due to the medium advance ratio used (μ=0.35), the wake is convected quite fast from the rotor disk, so a large number of mesh points are required at the background mesh level $\approx$ 50M (see Table 2).

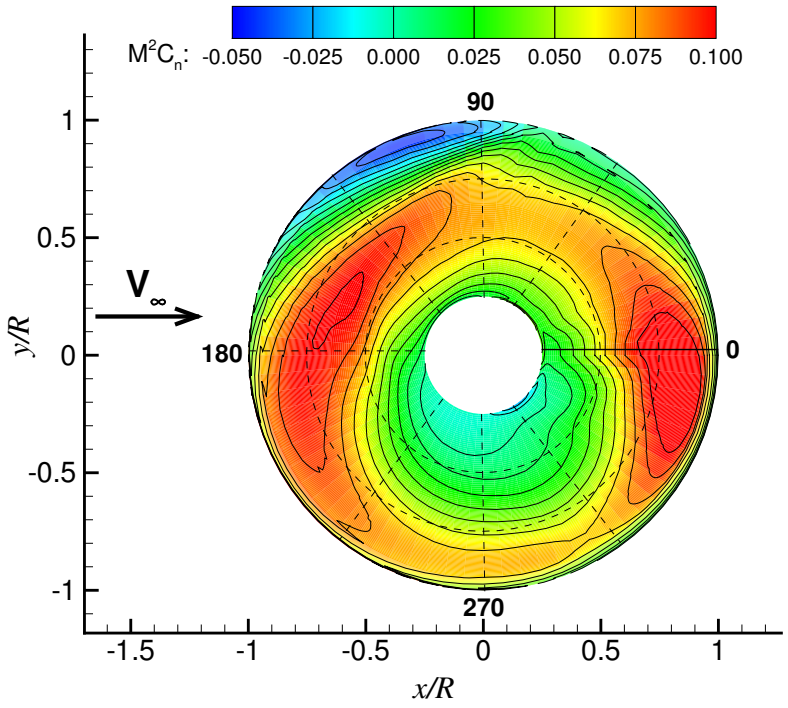

(a) M^2Cn.

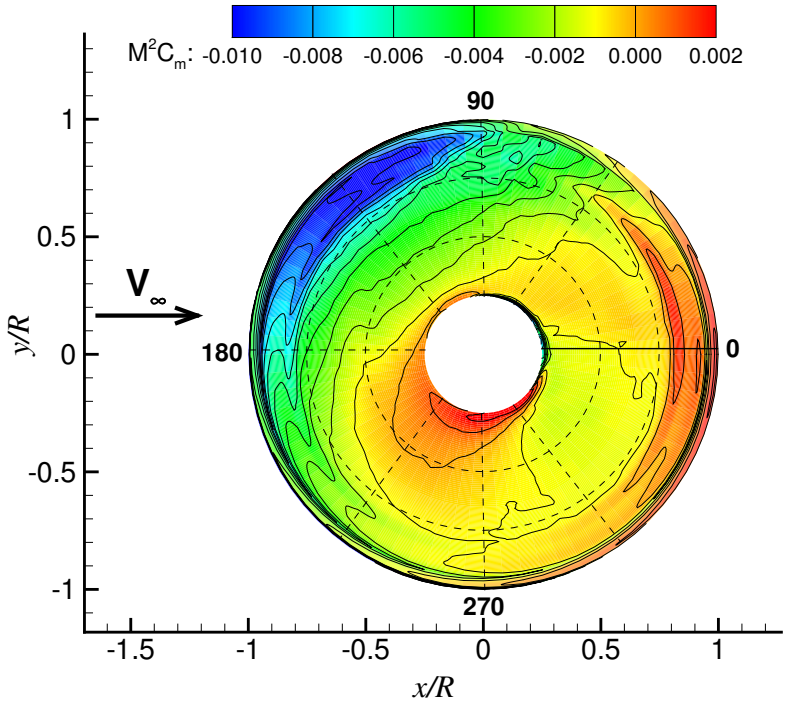

(b) M^2Cm.

Fig. 12: Rotor disk airloads (a) normal force and (b) pitching moment coefficients for the PSP rotor in forward flight at advance ratio μ=0.35 and C_T=0.006.

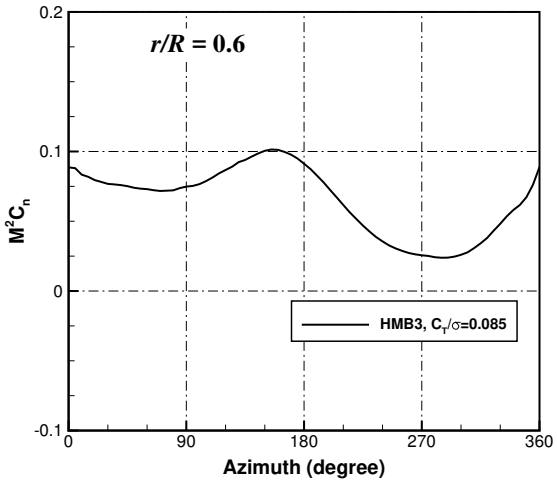

(a) r/R= 0.6.

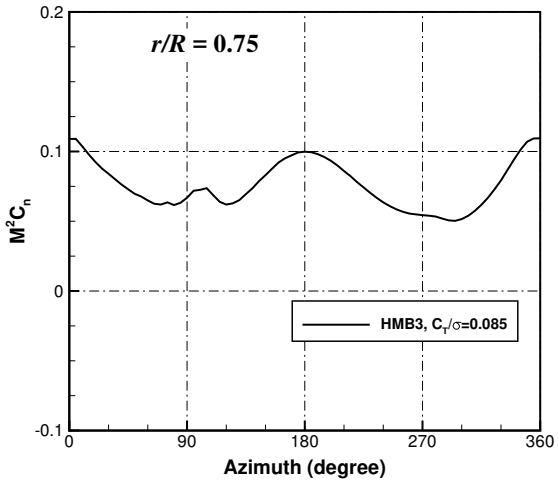

(b) r/R= 0.75.

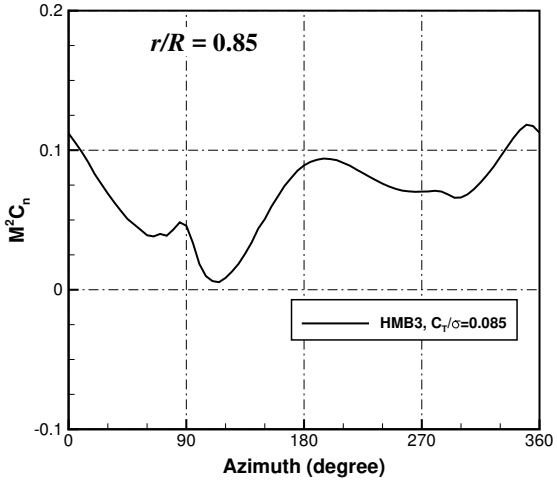

(c) r/R= 0.85.

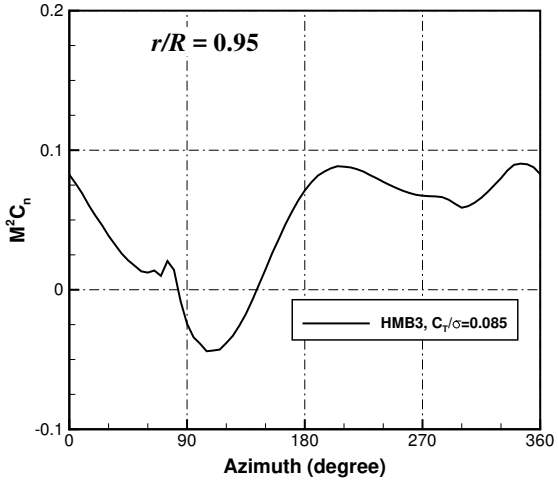

(d) r/R= 0.95.

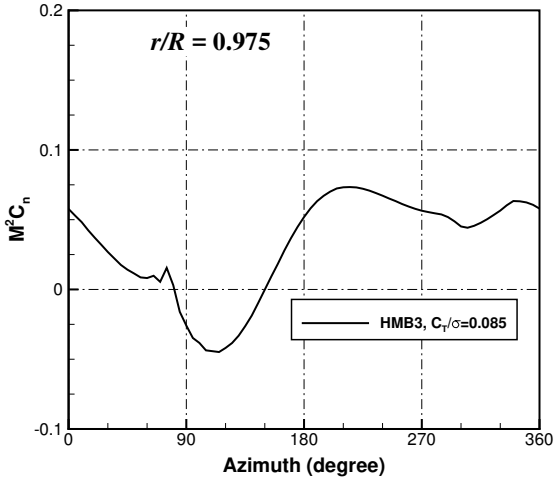

(e) r/R= 0.975.

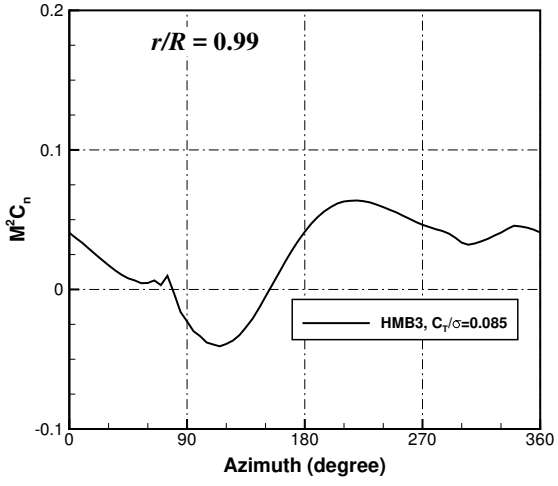

(f) r/R= 0.99.

Fig. 13: Predicted normal coefficient for the PSP rotor at advance ratio μ=0.35 and C_T=0.006 at six radial stations.

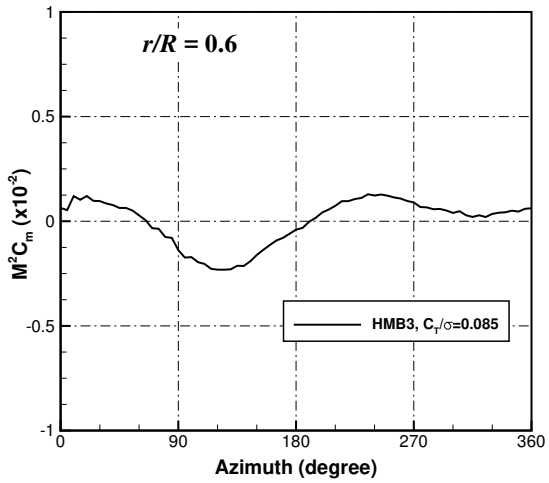

(a) r/R= 0.6.

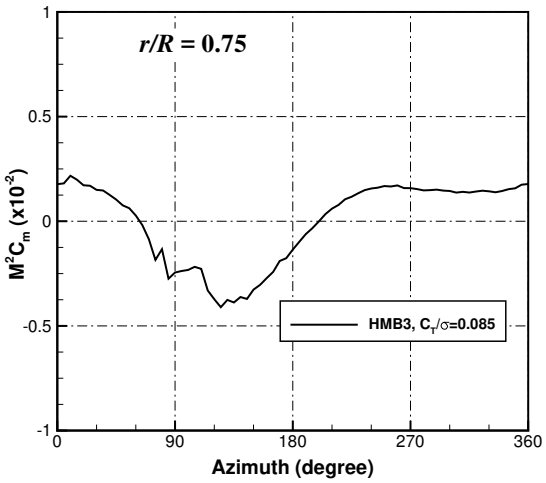

(b) r/R= 0.75.

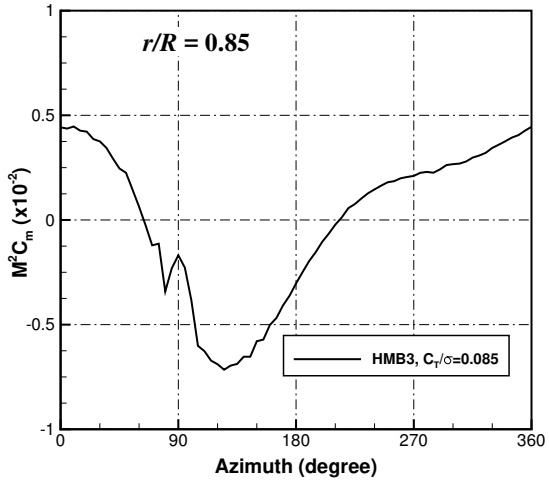

(c) r/R= 0.85.

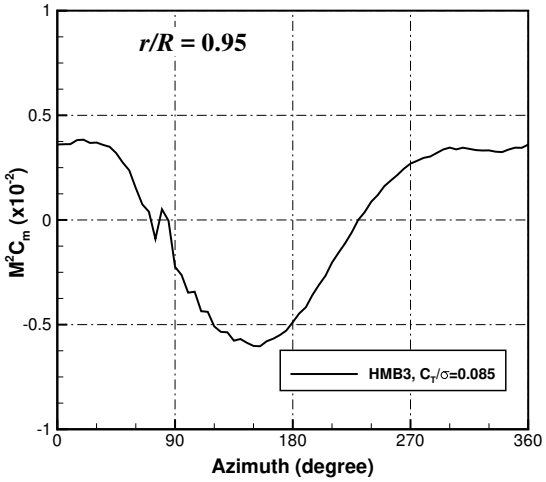

(d) r/R= 0.95.

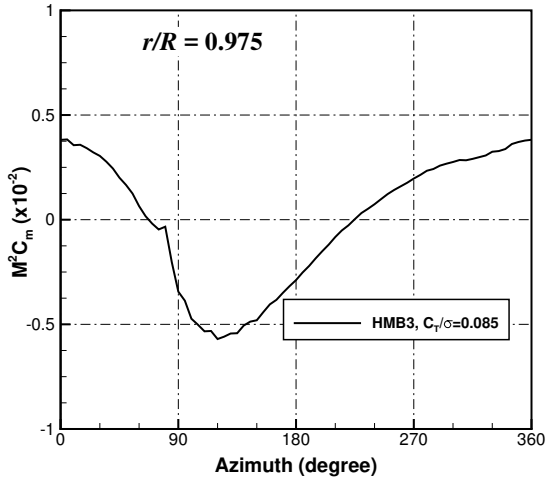

(e) r/R= 0.975.

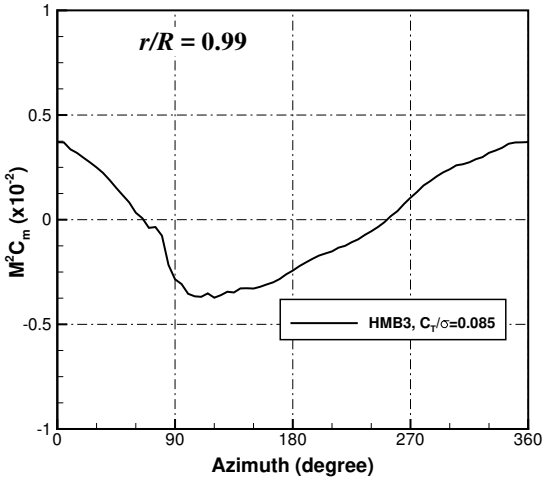

(f) r/R= 0.99.

Fig. 14: Predicted pitching moment (with mean values removed) for the PSP rotor at advance ratio μ= 0.35 and C_T=0.006 at six radial stations.

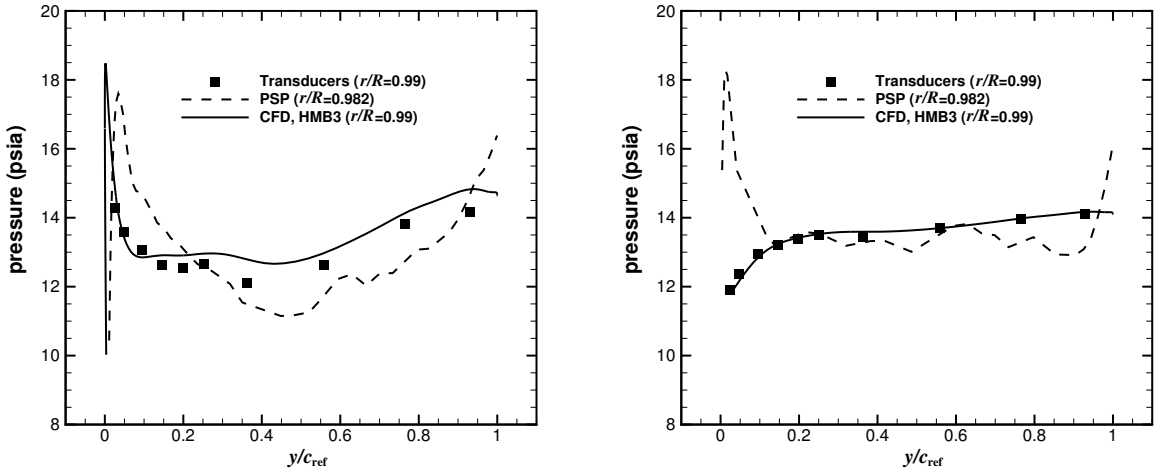

(a) ABS $\Psi = 101°$.

(b) RBS $\Psi = 262°$.

Fig. 15: C_P profile comparisons between experimental data using the PSP technique (dashed line) and pressure tap (square symbols) [3, 4] and CFD (solid line) at radial station $r/R = 0.99$. PSP rotor at advance ratio μ=0.35 and C_T=0.006 (a) ABS $\Psi = 101°$ and (b) RBS $\Psi = 262°$.

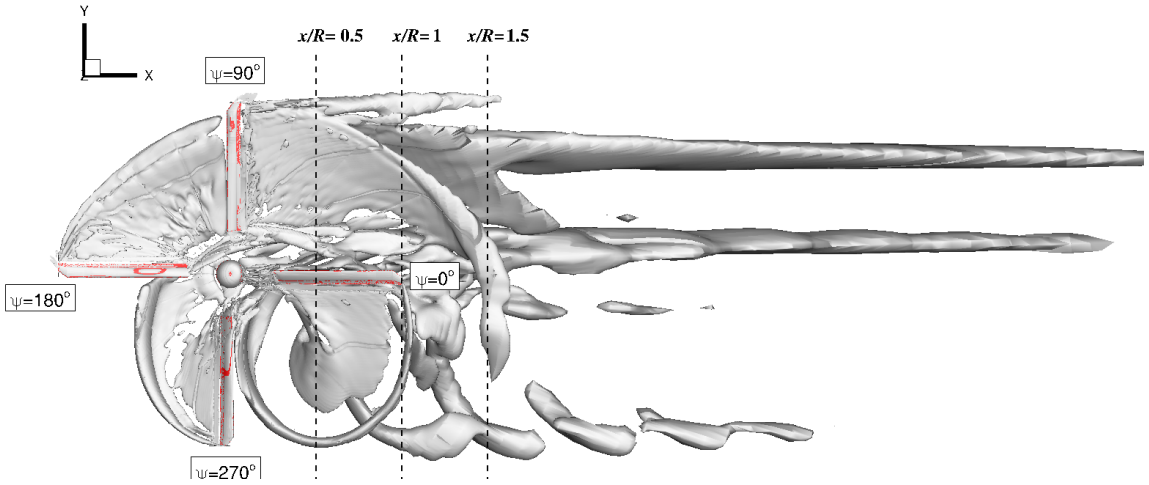

Fig. 16: Wake-visualisation of the PSP rotor in forward flight at advance ratio μ= 0.35 and C_T=0.006 using $\tilde{Q}$-criterion ($\tilde{Q}$=0.002).

VI. Conclusions

Fully turbulent flow solutions were obtained for the PSP blade in hover and forward flight. In hover, CFD results compare well with test data for the integrated blade load and surface pressure coefficient at blade-tip Mach number of 0.585. Regarding the PSP blade results at blade-tip Mach number of 0.65, experimental data is necessary for detailed comparisons. The agreement with the theory and published CFD works for the integrated loads is, however, encouraging. In forward flight, HMB results show a better agreement when compared with the C_P data obtained with the transducers Kulite than with the PSP technique.

As a future work, this study needs to be extended to include a mesh density investigation and unsteady computations in addition to the steady-state results presented here to gain a better insight of the PSP blade. Also, the use of transport-based transition model with the use of high-order spatial scheme need to be considered to capture the evolution of the flow transition on the PSP blade.

Acknowledgements

Results were obtained using the EPSRC funded ARCHIE-WeSt High Performance Computer (`www.archie-west.ac.uk`), EPSRC grant no. EP/K000586/1.

[1] Jimenez-Garcia, A. and Barakos, G. N., "CFD Analysis of Hover Performance of Rotors at Full-and Model-Scale Conditions," *The Aeronautical Journal*, Vol. 120, No. 1, 2016, pp. 1386–1424, DOI: 10.1017/aer.2016.58.

[2] Jimenez-Garcia, A. and Barakos, G. N., "Accurate Predictions of Rotor Hover Performance at Low and High Disc Loadings," *Journal of Aircraft*, Vol. 1, No. 1, 2017, pp. 1–12, DOI: 10.2514/1.C034144.

[3] Wong, O. D., Noonan, K. W., Watkins, A. N., Jenkins, L. N., and Yao, C. S., "Non-Intrusive Measurements of a Four-Bladed Rotor in Hover - A First Look," *Proceedings of the American Helicopter Society Aeromechanics Specialists*, AHS-2010, San Francisco, California, 2010, pp. 1–11.

[4] Wong, O. D., Watkins, A. N., Goodman, K. Z., Crafton, J., Forlines, A., Goss, L., Gregory, J. W., and Juliano, T. J., "Blade Tip Pressure Measurements using Pressure Sensitive Paint," *Proceedings of the 68th American Helicopter Society*, AHS-2012-000233, Fort Worth, Texas, 2012, pp. 1–14.

[5] Watkins, A. N., Leighty, B. D., Lipford, W. E., Goodman, K. Z., Crafton, J., and Gregory, J. W., "Measuring Surface Pressures on Rotor Blades Using Pressure-Sensitive Paint," *AIAA Journal*, Vol. 54, No. 1, 2016, pp. 206–215, DOI:http://dx.doi.org/10.2514/1.J054191.

[6] Overmeyer, A. D. and and, P. B. M., "Measured Boundary Layer Transition and Rotor Hover Performance at Model Scale," *Proceedings of the 55th Aerospace Sciences Meeting*, AIAA-2017-1872, Grapevine, Texas, 2017, pp. 1–36.

[7] Steijl, R., Barakos, G. N., and Badcock, K., "A framework for CFD analysis of helicopter rotors in hover and forward flight," *International Journal for Numerical Methods in Fluids*, Vol. 51, No. 8, 2006, pp. 819–847, DOI: 10.1002/d.1086.

[8] Steijl, R. and Barakos, G. N., "Sliding mesh algorithm for CFD analysis of helicopter rotor-fuselage aerodynamics," *International Journal for Numerical Methods in Fluids*, Vol. 58, No. 5, 2008, pp. 527–549, DOI: 10.1002/d.1757.

[9] Osher, S. and Chakravarthy, S., "Upwind schemes and boundary conditions with applications to Euler equations in general geometries," *Journal of Computational Physics*, Vol. 50, No. 3, 1983, pp. 447–481, DOI: 10.1016/0021-9991(83)90106-7.

[10] van Leer, B., "Towards the ultimate conservative difference scheme. V.A second-order sequel to Godunov's

Method," *Journal of Computational Physics*, Vol. 32, No. 1, 1979, pp. 101–136, DOI: 10.1016/0021-9991(79)90145-1.

[11] van Albada, G. D., van Leer, B., and Roberts, W. W., "A Comparative Study of Computational Methods in Cosmic Gas Dynamics," *Astronomy and Astrophysics*, Vol. 108, No. 1, 1982, pp. 76–84.

[12] Axelsson, O., *Iterative Solution Methods*, Cambridge University Press: Cambridge, MA, 1994.

[13] Wilcox, D., "Formulation of the k-omega Turbulence Model Revisited," *AIAA journal*, Vol. 46, No. 11, 2008, pp. 2823–2838, DOI: 10.2514/1.36541.

[14] Menter, F. R., "Two-Equation Eddy-Viscosity Turbulence Models for Engineering Applications," *AIAA Journal*, Vol. 32, No. 8, 1994, pp. 1598–1605, DOI: 10.2514/3.12149.

[15] Jarkowski, M., Woodgate, M., Barakos, G. N., and Rokicki, J., "Towards consistent hybrid overset mesh methods for rotorcraft CFD," *International Journal for Numerical Methods in Fluids*, Vol. 74, No. 8, 2014, pp. 543–576, DOI: 10.1002/fld.3861.

[16] Dehaeze, F. and Barakos, G. N., "Aeroelastic CFD Computations for Rotor Flows," *Proceedings of the Thirty-Seventh European Rotorcraft Forum*, ERF, Galarate, Italy, 2011, pp. 1–20.

[17] Jimenez, A. and Barakos, G. N., "Hover Predictions on the S-76 Rotor using HMB2," *Proceedings of the Fifty-Third Aerospace Sciences Meeting*, AIAA, Kissimmee, Florida, 2015, pp. 1–34.

[18] Gates, S., "Aerodynamic Analysis of Tiltrotors in Hovering and Propeller Modes Using Advanced Navier-Stokes Computations," *Proceedings of the Thirty-Ninth European Rotorcraft Forum*, ERF, Moscow, Russia, 2013, pp. 1–26.

[19] Noonan, K. W., "Aerodynamic Characteristics of Two Rotorcraft Airfoils Designed for Application to the Inboard Region of a Main Rotor Blade," NASA TP-3009, U.S. Army Aviation Systems Command, TR-90-B-005, July 1990.

[20] Noonan, K. W., "Aerodynamic Characteristics of Two Rotorcraft Airfoils Designed for Application to the Inboard Region of a Main Rotor Blade," NASA TM-4264, U.S. Army Aviation Systems Command, TR-91-B-003, May 1991.

[21] Gentry, G. L., Quinto, P. F., Gatlin, G. M., and Applin, Z. T., "The Langley 14- by 22-Foot Subsonic Tunnel," Description, Flow Characteristics and Guide for Users, NASA TP-3008, 1990.

[22] Wong, T.-C., "Application of CREATE^{TM}-AV Helios in an Engineering Environment: Hover Prediction Assessment," *Proceedings of the 55th Aerospace Sciences Meeting*, AIAA-2017-1667, Grapevine, Texas, 2017, pp. 1–26.

[23] Spalart, P. R. and Allmaras, S., "A One-Equation Turbulence Model for Aerodynamic Flows," *La Recherche Aérospatiale*, , No. 1, 1994, pp. 5–21.

[24] Vieira, B. A. O., Kinzel, M. P., and Maughmer, M. D., "CFD Hover Predictions Including Boundary-Layer Transition," *Proceedings of the 55th Aerospace Sciences Meeting*, AIAA-2017-1665, Grapevine, Texas, 2017, pp. 1–16.

[25] Rohit, J., "CFD Performance and Turbulence Transition Predictions on an Installed Model-scale Rotor in Hover," *Proceedings of the 55th Aerospace Sciences Meeting*, AIAA-2017-1871, Grapevine, Texas, 2017, pp. 1–29.

[26] Coder, J. G., "OVERFLOW Rotor Hover Simulations Using Advanced Turbulence and Transition Modeling," *Proceedings of the 55th Aerospace Sciences Meeting*, AIAA-2017-1432, Grapevine, Texas, 2017, pp. 1–19.

[27] Johnson, W., *Helicopter Theory*, Princeton University Press, New Jersey, 1980.

[28] Kocurek, J. D. and Tangler, J. L., "A Prescribed Wake Lifting Surface Hover Performance Analysis," *Journal of the American Helicopter Society*, Vol. 22, No. 1, 1977, pp. 24–35, DOI: 10.4050/JAHS.22.24.

[29] Landgrebe, A. J., "The Wake Geometry of a Hovering Rotor and its Influence on Rotor Performance," *Journal of the American Helicopter Society*, Vol. 17, No. 4, 1972, pp. 3–15, DOI: 10.4050/JAHS.17.3.

[30] Jeong, J. and Hussain, F., "On the Identification of a Vortex," *Journal of Fluid Mechanics*, Vol. 285, No. 1, 1995,

pp. 69–94, DOI: 10.1017/S0022112095000462.

[31] Potsdam, M., Yeo, H., and Johnson, W., "Rotor Airloads Prediction Using Loose Aerodynamic/Structural Coupling," *Proceedings of the 60th Annual Forum*, AHS, Baltimore, MD, 2004, pp. 1–22.